JOURNAL OF SPACECRAFT AND ROCKETS
Vol. 42, No. 4, July–August 2005

Dynamic Design of Octostrut Platform for Launch Stage Whole-Spacecraft Vibration Isolation

L. K. Liu,* L. Liang,† G. T. Zheng,‡ and W. H. Huang§
Harbin Institute of Technology, 150001 Harbin, People's Republic of China

Whole-spacecraft vibration isolation is a direct and effective approach to improving the dynamic environment that a spacecraft experiences during its journey to orbit. A method of analysis and dynamic design of an octostrut platform for whole-spacecraft vibration isolation during the launch stage is studied. Because the octostrut platform is a section between the launch vehicle and the spacecraft, structural characteristics of the launch vehicle and the spacecraft will inevitably influence the design of the isolation platform and also the vibration isolation effect, and vice versa. The design is divided into three parts. The first part is the preliminary analysis defining the fundamental parameters of the octostrut platform. In the second part, the parameters of each strut are defined by modeling the octostrut vibration isolation platform in a set of dynamic equations of motion. The third part is the coupling analysis, where finite element models of the octostrut platform, the spacecraft, and the launch vehicle are put together to assess the isolation effect and examine the influence of the isolation platform on the dynamic properties of the whole structure.

I. Introduction

THE launch stage is the most severe dynamic environment that a spacecraft will experience during its mission life. There are loads changing with environment, such as wind gusts and buffeting, and discrete events, such as motor ignitions and cutoffs, as well as variations in structural dynamics caused by fuel depletion and stage jettisons. To survive the launch stage, the structure of a spacecraft has to be strengthened by adding extra structural mass that will be useless in the operating orbit. This not only increases launch costs but also reduces the mass margin that could be used for launching additional payload.

Vibration isolation with an isolator, which is a mechanical interface in the vibration propagation path that acts as a mechanical low-pass filter providing low-frequency support that permits desired forces and torques to pass across the interface but rejects vibrations at higher frequencies, is an effective structural control technique for improving the dynamic environment. The idea of whole-spacecraft vibration isolation (WSVI) is to put an isolator into or use it to replace a payload attachment fitting (PAF), which is a section connecting the launch vehicle (LV) and the spacecraft together and traditionally is designed to be very stiff and provide an efficient transmission path for both dynamic and quasi-static launch loads. The concept of WSVI has been worked on since 1993, and to date, as reported publicly, there have been at least six successful flights with different WSVI systems.[1–4]

A number of researchers have investigated the use of Stewart platforms (or hexapods) for vibration isolation and precise pointing. For space applications Stewart platforms have the inherent capability of providing articulation between subsystems as well as vibration isolation with the same mechanical system. Consequently system complexity and weight can be significantly reduced. This also is convenient for system modeling and dynamic analysis.[5–8] However, the Stewart platform is a statically determinate structure; if any strut has a fault, disaster could be unavoidable. To meet high requirements for reliability in space applications, it is desired that redundancy should be provided by adding more struts to the platform. One approach is to use an octostrut platform that has eight struts. In addition to enhancing reliability, compared to a Stewart platform, it can also be designed with higher strength for heavy loads.

In the present paper, analysis and dynamic design methods for an octostrut passive vibration isolation platform for whole-spacecraft vibration isolation is studied. The design can be divided into three parts. The first part is the preliminary analysis for acquiring the fundamental parameters of the octostrut platform. The loads suffered during the ascent of the launch vehicle are also modeled to predict the performance of the platform with chosen fundamental parameters. The second part is the definition of parameters of each strut for the actual design. This is realized by modeling the octostrut platform as a set of dynamic equations of motion. The third part is a coupling dynamic analysis examining the performance of the platform and its influence on dynamic properties of the launch vehicle in practical applications. In this part, finite element models (FEMs) of the octostrut platform, the spacecraft, and the launch vehicle are put together as a whole structure.

II. Preliminary Analysis

The octostrut platform is a section between the launch vehicle and the spacecraft. Structural characteristics of the launch vehicle and the spacecraft will inevitably influence the design of the isolation platform and also the vibration isolation effect. Therefore, coupling analysis with the LV and the spacecraft is necessary for selecting proper parameters for the whole platform. Although complicated FEMs can give results with high precision and detail, in a stage of preliminary design, the finite element approach is neither easy to handle nor cost-effective for computation. Following the tradition of studying vibration isolation with a lumped parameter model of a few degrees of freedom (DOF), a 5-DOF lumped parameter model[9,10] is used here to carry out the preliminary analysis for the parameter selection.

The LV studied as an example in this paper is a three-stage rocket, whose fundamental parameters are listed in Table 1. During operation of the first stage, events include ignition, transonic flight, and maximum dynamic pressure. For the spacecraft, this is the severest load condition during the whole flight. The system at this duration

Received 19 May 2004; revision received 22 August 2004; accepted for publication 30 August 2004.

*Ph.D. Candidate, P.O. Box 137, Department of Space Engineering and Applied Mechanics; liulk@hit.edu.cn.
†Ph.D. Candidate, P.O. Box 137, Department of Space Engineering and Applied Mechanics; lianglu@hit.edu.cn.
‡Professor, P.O. Box 137, Department of Space Engineering and Applied Mechanics; gtzhengtu@yahoo.co.uk.
§Professor, P.O. Box 137, Department of Space Engineering and Applied Mechanics; whhuang@hit.edu.cn.

Table 1 Fundamental parameters of a launch vehicle

Parameter	First	Second	Third	PLE
Length, m	24.0	11.53	10.644	8.887
Diameter, m	3.35	3.35	3	3.75
Total mass, kg	175.680e3	31.906e3	19.400e3	500
Propellant mass, kg	170.000e3	29.600e3	17.600e3	
Case mass, kg	5.680e3	2.306e3	1.800e3	
Nozzle mass, kg	795.3	235.4	118.7	
Mass flow rate, kg/s	−1349.18	−259.65	−37.53	
Burn time, s	126	114	469	
Sea-level thrust, kN	2961.6			
Vacuum thrust, kN	3298.5	742.04	156.9	

Table 2 Fundamental parameters of a spacecraft

Length	Diameter	Total mass	Inertia tensor (at gravity center in $\{P\}$)
2.76 m	3.3 m (max)	2656 kg	$\begin{bmatrix} 2316.001 & 60.05046 & 4.460034 \\ 60.05046 & 2182.740 & -3.14755 \\ 4.460034 & -3.14755 & 1514.959 \end{bmatrix}$

will be simulated. Table 2 is a list of fundamental parameters of a spacecraft.

To get the loads, the orbit dynamic model must be built first. Then the vibration model will be built along this nominal orbit. In fact, the orbit dynamics of the LV with control during launch is complex. For simplicity and with the aim of demonstrating the procedure, a simple axial-orbit dynamic model without control is used here. Furthermore, the earth is assumed to be spherical and nonrotating, and the thrust and aerodynamic force are along the axial direction of the LV. With these assumptions, according to Ref. 11, the nominal-orbit dynamic equation is

$$m_c\dot{v}_c = (T + N_M) - (D + N_A) - m_c g\sin\alpha$$

$$v_c\dot{\alpha} = \frac{v_c^2\cos\alpha}{R_\oplus + v_c\sin\alpha} - g\cos\alpha, \qquad \frac{\mathrm{d}m_c}{\mathrm{d}t} = \dot{m}_c \tag{1}$$

where m_c is the instantaneous total mass of the system, v_c is the centroidal velocity of the system, D is the quasi-static drag force of the atmosphere, N_A is aeroacoustic-generated vibration, T is the quasi-static thrust of the engine, N_M is the engine-generated vibration, α is the flight path angle, which indicates the direction of the velocity vector with respect to the local horizon, and $R_\oplus$ is the radius of the earth.

During the launch, thrust increases with altitude because of atmospheric pressure decrease, and it is exponentially shut down in the last 6 s of operation. According to Ref. 10, the thrust is expressed as

$$T = \begin{cases} T_{S1} + (1 - P/101325)(T_{V1} - T_{S1}), & 0 \le t < (t_1 - 6) \\ [T_{S1} + (1 - P/101325)(T_{V1} - T_{S1})]e^{-[t-(t_1-6)]}, & (t_1 - 6) \le t < t_1 \end{cases} \tag{2}$$

where T_{S1} and T_{V1} are the thrust of the first-stage engine at sea level and in vacuum, respectively; P is the pressure of the atmosphere; and t_1 is the burnout time of the first stage. The quasi-static drag force of the atmosphere is

$$D = c_D\tfrac{1}{2}\rho\dot{v}_c^2 A \tag{3}$$

where c_D is the drag coefficient, ρ is the density of the atmosphere, and A is the effective area.

Two types of loads, other than the quasi-static loads, are considered here. They are engine-generated vibration and aeroacoustic-generated vibration. The engine-generated vibration source is at the nozzle of the operating stage. It includes a random band-limited white noise component and a resonant burn component. The resonant burn component is assigned a frequency and amplitude that are representative of the motor being considered. The band-limited white noise component is also assigned a magnitude that results in an appropriate level of vibration at the PAF. Aeroacoustic-generated vibration is related to the temperature of the atmosphere. To simplify the problem, the atmosphere is assumed to be isothermal.

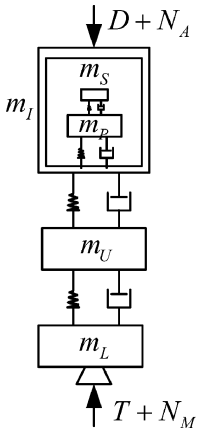

Fig. 1 Simplified dynamic model of launch vehicle–platform–spacecraft structure.

The LV is divided into three parts: the lower (L) and upper (U) components of the operating stage and the inert (I) component comprising the remaining stages of the LV (including the fairing) that are not burned. Considering the fuel consumption, the mass of each part is calculated from Table 1. Referring to the FEM of the LV, the connecting stiffness is calculated to capture two axial modes. The spacecraft is modeled as a rigid body with one axially moving part that is used to capture a mode of the spacecraft. The spacecraft's DOF is referred as the payload (P) component and the spacecraft subcomponent is referred as the subcomponent (S). The isolation platform is modeled as a spring parallel with a damper. The stiffness of the spring and the damping coefficient of the damper are expressed by the resonant frequency and the damping ratio of a system comprising the platform and the spacecraft. Figure 1 shows the dynamic model of the LV–platform–spacecraft structure, in which m_j ($j \in \{L, U, I, P, S\}$) represents the mass of component j. Along the nominal orbit, the vibration equation can be built as

$$\begin{aligned}
&m_L\ddot{x}_L + C_{LU} + K_{LU} \\
&\quad = (1 - m_L/m_c)(T + N_M) + (m_L/m_c)(D + N_A) \\
&m_U\ddot{x}_U + C_{UI} + C_{UL} + K_{UI} + K_{UL} \\
&\quad = -(m_U/m_c)(T + N_M - D - N_A) \\
&m_I\ddot{x}_I + C_{IP} + C_{IU} + K_{IP} + K_{IU} \\
&\quad = -(m_I/m_c)(T + N_M) + (1 - m_I/m_c)(-D - N_A) \\
&m_P\ddot{x}_P + C_{PS} + C_{PI} + K_{PS} + K_{PI} \\
&\quad = -(m_P/m_c)(T + N_M - D - N_A) \\
&m_S\ddot{x}_S + C_{SP} + K_{SP} = -(m_S/m_c)(T + N_M - D - N_A)
\end{aligned} \tag{4}$$

where m_i is the transient mass of the component i, x_i is the displacement of the component i relative to the centroid, $C_{ij} = c_{ij}(\dot{x}_i - \dot{x}_j)$, $K_{ij} = k_{ij}(x_i - x_j)$, k_{ij} is the stiffness of the spring connecting the component i and the component j, c_{ij} is the damping coefficient of the damper connecting the component i and the component j, $i \in \{L, U, I, P, S\}$, and $j \in \{L, U, I, P, S\}$.

The resonant frequency and the damping ratio are important parameters of an isolator. With different resonant frequencies and damping ratios of the platform, time histories of acceleration are calculated by solving the vibration equation [Eq. (4)]. Root-mean-square (rms) acceleration is calculated from the power spectrum density of these time histories and used to estimate the effect of

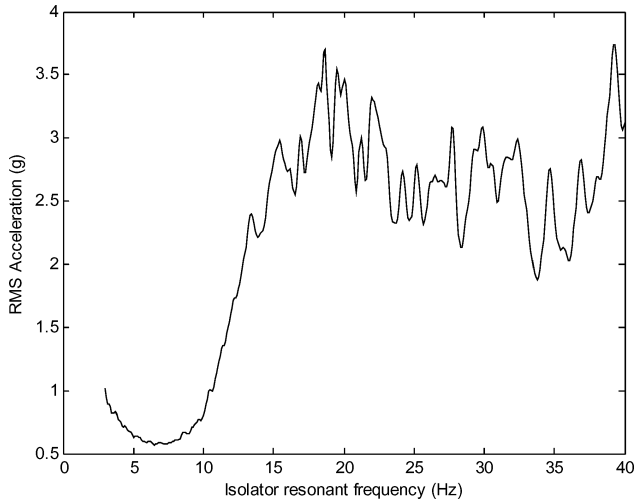

Fig. 2 RMS acceleration of the payload vs the resonant frequency.

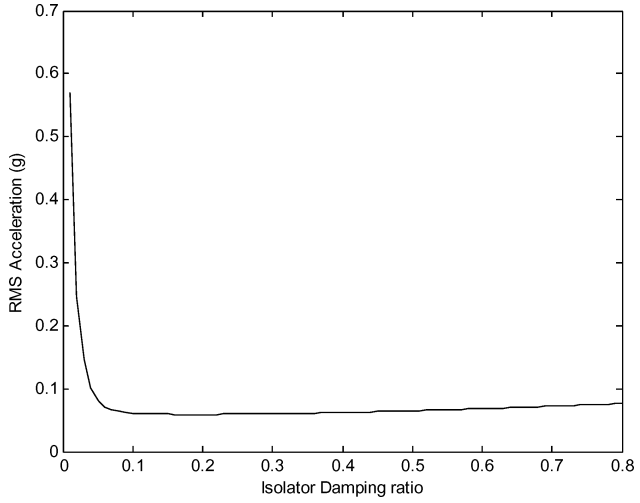

Fig. 3 RMS acceleration of the payload vs the damping ratio.

the isolator. When the resonant frequency of the isolator is changed from 3 to 40 Hz, Fig. 2 shows that at 6.5 Hz, the payload will suffer the least rms acceleration. The value is $0.569g$. Another important parameter of the isolator is the damping ratio. As showed in Fig. 3, with increased damping ratio, the rms acceleration of the payload first decreases and then increases slowly. At 0.19, the rms acceleration reaches its minimum value, which is $0.059g$. The reason is that a higher damping ratio helps to attenuate the resonant peak, but the transmissibility outside the $\sqrt{2}$ time range will be increased. So there exists an optimal damping ratio.

In Fig. 4, time histories of acceleration during the first stage working below the isolator (black curve) and above the isolator (gray curve) are displayed. The resonant frequency of the isolator is 6.5 Hz, and the damping ratio is 0.01. The magnitude of vibration above the isolator just after the ignition (at the zero second) is large. In Fig. 5, when the damping ratio is changed to 0.19, the vibration just after the ignition is mitigated.

III. Dynamic Modeling and Parameter Definition

A typical octostrut vibration isolation platform (Fig. 6) consists of a rigid launch-vehicle interface (LVI), a rigid payload interface (PI), and eight flexible struts the length of which can be changed along their axial direction. Connections of a strut to the LVI and the PI are spherical joints. Neglecting the gravity and inertial force of the strut, all forces transmitted through a strut are axial forces. This means that for a single strut, the original six-axis vibration isolation problem can be turned into a single-axis vibration isolation problem. This helps to simplify the design of the single strut and further the whole vibration isolation platform design.

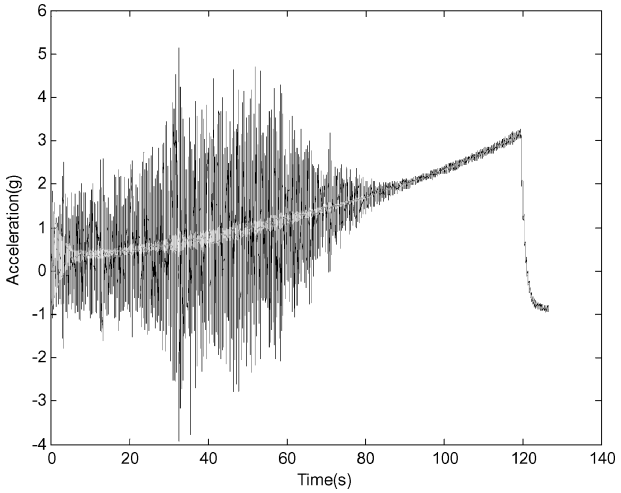

Fig. 4 Acceleration below and above the isolator (resonant frequency 6.5 Hz; damping ratio 0.01).

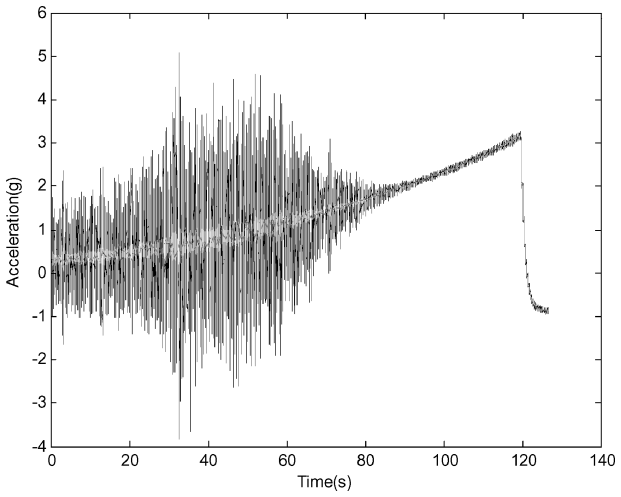

Fig. 5 Acceleration below and above the isolator (resonant frequency 6.5 Hz; damping ratio 0.19).

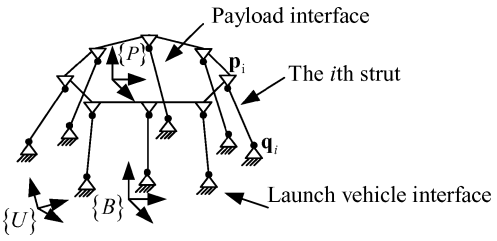

Fig. 6 General octostrut vibration isolation platform.

A. Kinematics of the Platform

Three Cartesian reference frames are used in this paper. $\{P\}$ is a reference frame located at, and rigidly attached to, the PI and payload's center of mass. $\{B\}$ is a reference frame attached to the LVI. $\{U\}$ is a universal inertial reference frame. For a position, velocity, or acceleration vector, a left superscript denotes the frame, relative to the origin of which the vector is measured.

Let $\boldsymbol{p}_i$ denote the central position of the ith joint that connects the PI and the ith strut; then

$$^{U}\boldsymbol{p}_i = {}^{U}\boldsymbol{x}_P + {}^{P}\boldsymbol{p}_i \tag{5}$$

$$^{U}\dot{\boldsymbol{p}}_i = {}^{U}\boldsymbol{v}_P + {}^{U}\boldsymbol{\omega}_P \times {}^{P}\boldsymbol{p}_i \tag{6}$$

$$^{U}\ddot{\boldsymbol{p}}_i = {}^{U}\dot{\boldsymbol{v}}_P + {}^{U}\dot{\boldsymbol{\omega}}_P \times {}^{P}\boldsymbol{p}_i + \boldsymbol{c}_{1i} \tag{7}$$

where ${}^{U}\boldsymbol{x}_P$ is the position vector from the origin of $\{U\}$ to the origin of $\{P\}$, ${}^{U}\boldsymbol{v}_P = {}^{U}\dot{\boldsymbol{x}}_P$, ${}^{U}\boldsymbol{\omega}_P$ is the angular velocity of $\{P\}$ with respect to $\{U\}$, and $\boldsymbol{c}_{1i} = {}^{U}\boldsymbol{\omega}_P \times ({}^{U}\boldsymbol{\omega}_P \times {}^{P}\boldsymbol{p}_i)$. Let ${}^{U}\boldsymbol{X}_P = [{}^{U}\boldsymbol{x}_P \;\; {}^{U}\boldsymbol{\theta}_P]^T$, where ${}^{U}\boldsymbol{\theta}_P$ is the Cardan angle that depicts the attitude of $\{P\}$ with respect to $\{U\}$, ${}^{U}\bar{\boldsymbol{\theta}}_P = [\theta_{Px} \;\; \theta_{Py} \;\; \theta_{Pz}]^T$; then

$$ {}^{U}\bar{\boldsymbol{\omega}}_P = \bar{A}({}^{U}\bar{\boldsymbol{\theta}}_P){}^{U}\dot{\bar{\boldsymbol{\theta}}}_P \tag{8} $$

where

$$ \bar{A}\left({}^{U}\boldsymbol{\theta}_P\right) = \begin{bmatrix} \cos\theta_{Py}\cos\theta_{Pz} & \sin\theta_{Pz} & 0 \\ -\cos\theta_{Py}\sin\theta_{Pz} & \cos\theta_{Pz} & 0 \\ \sin\theta_{Py} & 0 & 1 \end{bmatrix} $$

Let $\boldsymbol{q}_i$ denote the central position of the ith joint connecting the LVI and the ith strut. Then

$$ {}^{U}\boldsymbol{q}_i = {}^{U}\boldsymbol{x}_B + {}^{B}\boldsymbol{q}_i \tag{9} $$

$$ {}^{U}\dot{\boldsymbol{q}}_i = {}^{U}\boldsymbol{v}_B + {}^{U}\omega_B \times {}^{B}\boldsymbol{q}_i \tag{10} $$

$$ {}^{U}\ddot{\boldsymbol{q}}_i = {}^{U}\dot{\boldsymbol{v}}_B + {}^{U}\dot{\boldsymbol{\omega}}_B \times {}^{B}\boldsymbol{q}_i + \boldsymbol{c}_{2i} \tag{11} $$

where ${}^{U}\boldsymbol{x}_B$ is the position vector from the origin of $\{U\}$ to the origin of $\{B\}$, ${}^{U}\boldsymbol{v}_B = {}^{U}\dot{\boldsymbol{x}}_B$, ${}^{U}\boldsymbol{\omega}_B$ is the angular velocity of $\{B\}$ with respect to $\{U\}$, and $\boldsymbol{c}_{2i} = {}^{U}\boldsymbol{\omega}_B \times ({}^{U}\boldsymbol{\omega}_B \times {}^{B}\boldsymbol{q}_i)$. Let ${}^{U}\boldsymbol{X}_B = [{}^{U}\boldsymbol{x}_B \;\; {}^{U}\boldsymbol{\theta}_B]^T$, where ${}^{U}\boldsymbol{\theta}_B$ is the Cardan angle that depicts the attitude of $\{B\}$ with respect to $\{U\}$; then

$$ {}^{U}\bar{\boldsymbol{\omega}}_B = \bar{A}({}^{U}\bar{\boldsymbol{\theta}}_B){}^{U}\dot{\bar{\boldsymbol{\theta}}}_B \tag{12} $$

Define the strut vector as

$$ \boldsymbol{w}_i = {}^{U}\boldsymbol{p}_i - {}^{U}\boldsymbol{q}_i \tag{13} $$

then the length of the strut and the unit vector along the strut are

$$ l_i = \|\boldsymbol{w}_i\|, \qquad \boldsymbol{u}_i = \boldsymbol{w}_i / l_i \tag{14} $$

The elongation velocity of the strut is given as

$$ \dot{l}_i = \boldsymbol{u}_i \cdot \dot{\boldsymbol{w}}_i = \boldsymbol{u}_i \cdot \left({}^{U}\dot{\boldsymbol{p}}_i - {}^{U}\dot{\boldsymbol{q}}_i\right) = \boldsymbol{u}_i \cdot {}^{U}\boldsymbol{v}_P + {}^{P}\boldsymbol{p}_i \times \boldsymbol{u}_i $$

$$ \cdot {}^{U}\boldsymbol{\omega}_P - \boldsymbol{u}_i \cdot {}^{U}\boldsymbol{v}_B - {}^{B}\boldsymbol{q}_i \times \boldsymbol{u}_i \cdot {}^{U}\boldsymbol{\omega}_B \tag{15} $$

The acceleration of the strut vector can be expressed in terms of the strut's elongation acceleration $\ddot{l}_i$, angular velocity $\boldsymbol{\omega}_{li}$, and angular acceleration ε_{li} as

$$ \ddot{\boldsymbol{w}}_i = \varepsilon_{li} \times \boldsymbol{w}_i + \omega_{li} \times (\omega_{li} \times \boldsymbol{w}_i) + \ddot{l}_i \boldsymbol{u}_i + 2\omega_{li} \times \dot{l}_i \boldsymbol{u}_i \tag{16} $$

Assume that the strut is symmetric about its axis, and there is no moment input along the axis of the strut, so that $\boldsymbol{u}_i \cdot \boldsymbol{\omega}_{li} = 0$ and $\boldsymbol{u}_i \cdot \varepsilon_{li} = 0$. Equation (16) can be changed into

$$ \ddot{\boldsymbol{w}}_i = \varepsilon_{li} \times \boldsymbol{w}_i + (\ddot{l}_i - l_i \omega_{li} \cdot \omega_{li})\boldsymbol{u}_i + 2\omega_{li} \times \dot{l}_i \boldsymbol{u}_i \tag{17} $$

Now by dot product with $\boldsymbol{u}_i$, the elongation acceleration of the ith strut can be expressed as

$$ \ddot{l}_i = \boldsymbol{u}_i \cdot \ddot{\boldsymbol{w}}_i + l_i \omega_{li} \cdot \omega_{li} = \boldsymbol{u}_i \cdot {}^{U}\dot{\boldsymbol{v}}_P + {}^{P}\boldsymbol{p}_i \times \boldsymbol{u}_i \cdot {}^{U}\dot{\boldsymbol{\omega}}_P $$

$$ - \boldsymbol{u}_i \cdot {}^{U}\dot{\boldsymbol{v}}_B - {}^{B}\boldsymbol{q}_i \times \boldsymbol{u}_i \cdot {}^{U}\dot{\boldsymbol{\omega}}_B + c_{3i} \tag{18} $$

where $c_{3i} = \boldsymbol{u}_i \cdot (\boldsymbol{c}_{1i} - \boldsymbol{c}_{2i}) + l_i \omega_{li} \cdot \omega_{li}$.

The acceleration of the upper end of the strut can also expressed as

$$ {}^{U}\ddot{\boldsymbol{p}}_i = {}^{U}\ddot{\boldsymbol{q}}_i + \varepsilon_{li} \times \boldsymbol{w}_i + \omega_{li} \times (\omega_{li} \times \boldsymbol{w}_i) + \ddot{l}_i \boldsymbol{u}_i + 2\omega_{li} \times \dot{l}_i \boldsymbol{u}_i \tag{19} $$

From Eq. (19), there is

$$ \boldsymbol{u}_i \cdot {}^{U}\ddot{\boldsymbol{p}}_i = \boldsymbol{u}_i \cdot {}^{U}\ddot{\boldsymbol{q}}_i + \ddot{l}_i + c_{4i} \tag{20} $$

where $c_{4i} = \boldsymbol{u}_i \cdot [\omega_{li} \times (\omega_{li} \times \boldsymbol{w}_i)]$.

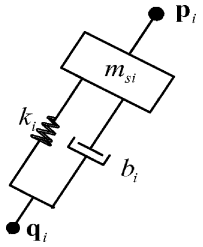

Fig. 7 Dynamic model of the *i*th strut.

B. Dynamics of the Platform

Figure 7 shows the dynamic model of the ith strut. Here m_{si} is the strut moving mass, k_i is the spring stiffness, and b_i is the damping coefficient. Applying Newton's second law for the ith strut,

$$ m_{si}\boldsymbol{u}_i \cdot {}^{U}\ddot{\boldsymbol{p}}_i = -f_{Pi} - m_{si}\boldsymbol{u}_i \cdot \boldsymbol{g} - k_i(l_i - l_{0i}) - b_i\dot{l}_i \tag{21} $$

where f_{Pi} is the force on the strut from the PI and l_{0i} denotes the relaxed strut length. According to Eq. (20), Eq. (21) can be transformed into

$$ f_{Pi} = -m_{si}\ddot{l}_i - m_{si}\boldsymbol{u}_i \cdot {}^{U}\ddot{\boldsymbol{q}}_i - k_i(l_i - l_{0i}) - b_i\dot{l}_i - m_{si}\boldsymbol{u}_i \cdot \boldsymbol{g} - m_{si}c_{4i} \tag{22} $$

For all of the struts,

$$ \bar{\boldsymbol{f}}_P = -\bar{\boldsymbol{M}}_s\ddot{\bar{\boldsymbol{l}}} - \bar{\boldsymbol{K}}(\bar{\boldsymbol{l}} - \bar{\boldsymbol{l}}_0) - \bar{\boldsymbol{B}}\dot{\bar{\boldsymbol{l}}} - \bar{\boldsymbol{M}}_s{}^{U}\ddot{\bar{\boldsymbol{q}}}_u - \bar{\boldsymbol{M}}_s\bar{\boldsymbol{g}}_u - \bar{\boldsymbol{c}}_4 \tag{23} $$

where

$$ \bar{\boldsymbol{f}}_p = [f_{p1} \quad f_{p2} \quad \cdots \quad f_{pN}]^T, \qquad \bar{\boldsymbol{l}} = [l_1 \quad l_2 \quad \cdots \quad l_N]^T $$

$$ \bar{\boldsymbol{l}}_0 = [l_{01} \quad l_{02} \quad \cdots \quad l_{0N}]^T $$

$$ \bar{\boldsymbol{M}}_s = \mathrm{diag}([m_{s1} \quad m_{s2} \quad \cdots \quad m_{sN}]) $$

$$ \bar{\boldsymbol{K}} = \mathrm{diag}([k_1 \quad k_2 \quad \cdots \quad k_N]) $$

$$ \bar{\boldsymbol{B}} = \mathrm{diag}([b_1 \quad b_2 \quad \cdots \quad b_N]) $$

$$ {}^{U}\bar{\boldsymbol{q}}_u = \left[\bar{\boldsymbol{u}}_1^T{}^{U}\bar{\boldsymbol{q}}_1 \quad \bar{\boldsymbol{u}}_2^T{}^{U}\bar{\boldsymbol{q}}_2 \quad \cdots \quad \bar{\boldsymbol{u}}_N^T{}^{U}\bar{\boldsymbol{q}}_N\right]^T $$

$$ \bar{\boldsymbol{g}}_u = \left[\bar{\boldsymbol{u}}_1^T\bar{\boldsymbol{g}} \quad \bar{\boldsymbol{u}}_2^T\bar{\boldsymbol{g}} \quad \cdots \quad \bar{\boldsymbol{u}}_N^T\bar{\boldsymbol{g}}\right]^T $$

$$ \bar{\boldsymbol{c}}_4 = [m_{s1}c_{41} \quad m_{s2}c_{42} \quad \cdots \quad m_{sN}c_{4N}]^T $$

According to Eq. (15),

$$ \dot{\bar{\boldsymbol{l}}} = \bar{\boldsymbol{J}}_P{}^{U}\dot{\bar{\boldsymbol{X}}}_{P1} - \bar{\boldsymbol{J}}_B{}^{U}\dot{\bar{\boldsymbol{X}}}_{B1} \tag{24} $$

where

$$ \bar{\boldsymbol{J}}_P = \begin{pmatrix} \bar{\boldsymbol{u}}_1^T & \left({}^{P}\tilde{\boldsymbol{p}}_1\bar{\boldsymbol{u}}_1\right)^T \\ \vdots & \vdots \\ \bar{\boldsymbol{u}}_N^T & \left({}^{P}\tilde{\boldsymbol{p}}_N\bar{\boldsymbol{u}}_N\right)^T \end{pmatrix}, \qquad \dot{\bar{\boldsymbol{X}}}_{P1} = \begin{bmatrix} {}^{U}\dot{\boldsymbol{x}}_P \\ \bar{A}\left({}^{U}\bar{\boldsymbol{\theta}}_P\right){}^{U}\dot{\bar{\boldsymbol{\theta}}}_P \end{bmatrix} $$

$$ \bar{\boldsymbol{J}}_B = \begin{pmatrix} \bar{\boldsymbol{u}}_1^T & \left({}^{B}\tilde{\boldsymbol{q}}_1\bar{\boldsymbol{u}}_1\right)^T \\ \vdots & \vdots \\ \bar{\boldsymbol{u}}_N^T & \left({}^{B}\tilde{\boldsymbol{q}}_N\bar{\boldsymbol{u}}_N\right)^T \end{pmatrix}, \qquad \dot{\bar{\boldsymbol{X}}}_{B1} = \begin{bmatrix} {}^{U}\dot{\boldsymbol{x}}_B \\ \bar{A}\left({}^{U}\bar{\boldsymbol{\theta}}_B\right){}^{U}\dot{\bar{\boldsymbol{\theta}}}_B \end{bmatrix} $$

According to Eq. (18),

$$ \ddot{\bar{\boldsymbol{l}}} = \bar{\boldsymbol{J}}_P{}^{U}\ddot{\bar{\boldsymbol{X}}}_{P1} - \bar{\boldsymbol{J}}_B{}^{U}\ddot{\bar{\boldsymbol{X}}}_{B1} + \bar{\boldsymbol{c}}_3 \tag{25} $$

where

$$\ddot{\bar{\boldsymbol{X}}}_{P1} = \begin{bmatrix} {}^{U}\ddot{\boldsymbol{x}}_P \\ \bar{A}\left({}^{U}\bar{\boldsymbol{\theta}}_P\right){}^{U}\ddot{\boldsymbol{\theta}}_P \end{bmatrix}, \qquad \ddot{\bar{\boldsymbol{X}}}_{B1} = \begin{bmatrix} {}^{U}\ddot{\boldsymbol{x}}_B \\ \bar{A}\left({}^{U}\bar{\boldsymbol{\theta}}_B\right){}^{U}\ddot{\boldsymbol{\theta}}_B \end{bmatrix}$$

$$\bar{\boldsymbol{c}}_3 = \begin{bmatrix} c_{31} \\ \vdots \\ c_{3N} \end{bmatrix} + \bar{\boldsymbol{J}}_P \begin{bmatrix} 0_{3\times 1} \\ \dot{\bar{A}}\left({}^{U}\bar{\boldsymbol{\theta}}_P\right){}^{U}\dot{\bar{\boldsymbol{\theta}}}_P \end{bmatrix} - \bar{\boldsymbol{J}}_B \begin{bmatrix} 0_{3\times 1} \\ \dot{\bar{A}}\left({}^{U}\bar{\boldsymbol{\theta}}_B\right){}^{U}\dot{\bar{\boldsymbol{\theta}}}_B \end{bmatrix}$$

From Eq. (11),

$${}^{U}\ddot{\bar{\boldsymbol{q}}}_u = \bar{\boldsymbol{J}}_B{}^{U}\ddot{\bar{\boldsymbol{X}}}_{B1} + \bar{\boldsymbol{c}}_2 \tag{26}$$

where

$$\bar{\boldsymbol{c}}_2 = \begin{bmatrix} \bar{\boldsymbol{u}}_1^T\bar{\boldsymbol{c}}_{21} \\ \vdots \\ \bar{\boldsymbol{u}}_N^T\bar{\boldsymbol{c}}_{2N} \end{bmatrix} + \bar{\boldsymbol{J}}_B \begin{bmatrix} 0_{3\times 1} \\ \dot{\bar{A}}\left({}^{U}\bar{\boldsymbol{\theta}}_B\right){}^{U}\dot{\bar{\boldsymbol{\theta}}}_B \end{bmatrix}$$

From Eqs. (24–26),

$$\bar{\boldsymbol{f}}_P = -\bar{\boldsymbol{M}}_s\bar{\boldsymbol{J}}_P{}^{U}\ddot{\bar{\boldsymbol{X}}}_{P1} - \bar{\boldsymbol{B}}\bar{J}_P{}^{U}\dot{\bar{\boldsymbol{X}}}_{P1} + \bar{\boldsymbol{B}}\bar{J}_B{}^{U}\dot{\bar{\boldsymbol{X}}}_{B1} - \bar{\boldsymbol{K}}(\bar{\boldsymbol{l}} - \bar{\boldsymbol{l}}_0) - \bar{\boldsymbol{M}}_s\bar{\boldsymbol{g}}_u + \bar{\boldsymbol{c}}_5 \tag{27}$$

where $\bar{\boldsymbol{c}}_5 = -\bar{\boldsymbol{M}}_s\bar{\boldsymbol{c}}_3 - \bar{\boldsymbol{M}}_s\bar{\boldsymbol{c}}_2 - \bar{\boldsymbol{c}}_4$.

If the PI is modeled as a rigid body, Newton's equation for the PI can be written as

$$m_P\ddot{\boldsymbol{x}}_P = \sum_{i=1}^{N}\boldsymbol{u}_i f_{pi} + m_P\boldsymbol{g} + \boldsymbol{f}_e \tag{28}$$

where $\boldsymbol{f}_e$ represents force applied to the PI by the payload. Taking the moments about the center of mass of the PI, Euler's equations for the PI give

$$\boldsymbol{I}_P\dot{\boldsymbol{\omega}}_P + \boldsymbol{\omega}_P \times \boldsymbol{I}_P\boldsymbol{\omega}_P = \sum_{i=1}^{N}{}^{P}\boldsymbol{p}_i \times \boldsymbol{u}_i f_{pi} + \boldsymbol{M}_e \tag{29}$$

where $\boldsymbol{M}_e$ represents moment applied to the PI by the spacecraft. Putting Eqs. (28) and (29) together and changing the equations into matrix form yields

$$\bar{\boldsymbol{M}}\ddot{\bar{\boldsymbol{X}}}_{P1} = \bar{\boldsymbol{F}}_P + \bar{\boldsymbol{G}}_P + \bar{\boldsymbol{F}}_e + \bar{\boldsymbol{c}}_6 \tag{30}$$

where

$$\bar{\boldsymbol{M}} = \begin{bmatrix} m_P\bar{\boldsymbol{I}}_3 & 0 \\ 0 & \bar{\boldsymbol{I}}_P \end{bmatrix}, \qquad \bar{\boldsymbol{F}}_P = \begin{bmatrix} \sum_{i=1}^{N}\bar{\boldsymbol{u}}_i f_{pi} \\ \sum_{i=1}^{N}{}^{P}\tilde{\boldsymbol{p}}_i\bar{\boldsymbol{u}}_i f_{pi} \end{bmatrix} = \bar{\boldsymbol{J}}_P^T\bar{\boldsymbol{f}}_P$$

$$\bar{\boldsymbol{G}}_P = \begin{bmatrix} m_p\bar{\boldsymbol{g}} \\ 0 \end{bmatrix}, \qquad \bar{\boldsymbol{F}}_e = \begin{bmatrix} \bar{\boldsymbol{f}}_e \\ \bar{\boldsymbol{M}}_e \end{bmatrix}$$

$$\bar{\boldsymbol{c}}_6 = \begin{bmatrix} 0 \\ \tilde{\boldsymbol{\omega}}_P\bar{\boldsymbol{I}}_P\bar{\boldsymbol{\omega}}_P - \bar{\boldsymbol{I}}_P\dot{\bar{A}}\left({}^{U}\boldsymbol{\theta}_P\right){}^{U}\dot{\bar{\boldsymbol{\theta}}}_P \end{bmatrix}$$

From Eq. (27),

$$\left(\bar{\boldsymbol{M}} + \bar{\boldsymbol{J}}_P^T\bar{\boldsymbol{M}}_s\bar{\boldsymbol{J}}_P\right)\ddot{\bar{\boldsymbol{X}}}_{P1} + \bar{\boldsymbol{J}}_P^T\bar{\boldsymbol{B}}\bar{\boldsymbol{J}}_P{}^{U}\dot{\bar{\boldsymbol{X}}}_{P1} + \bar{\boldsymbol{J}}_P^T\bar{\boldsymbol{K}}(\bar{\boldsymbol{l}} - \bar{\boldsymbol{l}}_0) = \bar{\boldsymbol{J}}_P^T\bar{\boldsymbol{B}}\bar{\boldsymbol{J}}_B{}^{U}\dot{\bar{\boldsymbol{X}}}_{B1} + \bar{\boldsymbol{G}} + \bar{\boldsymbol{F}}_e + \bar{\boldsymbol{c}}_7 \tag{31}$$

where $\bar{\boldsymbol{G}} = \bar{\boldsymbol{G}}_P - \bar{\boldsymbol{J}}_P^T\bar{\boldsymbol{M}}_s\bar{\boldsymbol{g}}_u$, and $\bar{\boldsymbol{c}}_7 = \bar{\boldsymbol{c}}_6 + \bar{\boldsymbol{J}}_P^T\bar{\boldsymbol{c}}_5$. By letting spring compression absorb the static gravity force, $\bar{\boldsymbol{G}}$ can be removed from the equation.

For structural vibration of small amplitude, it can be assumed that the structure of the platform is not changed, and the velocity is also a small quantity; thus all second-order small quantities can be discarded. So ${}^{U}\dot{\bar{\boldsymbol{X}}}_{P1} \approx {}^{U}\dot{\bar{\boldsymbol{X}}}_P$, ${}^{U}\dot{\bar{\boldsymbol{X}}}_{P1} \approx {}^{U}\dot{\bar{\boldsymbol{X}}}_P$, ${}^{U}\dot{\bar{\boldsymbol{X}}}_{B1} \approx {}^{U}\dot{\bar{\boldsymbol{X}}}_B$, $\bar{\boldsymbol{c}}_7 \approx 0$, and

$$\bar{\boldsymbol{l}} - \bar{\boldsymbol{l}}_0 \approx \bar{\boldsymbol{J}}_P{}^{U}\bar{\boldsymbol{X}}_P - \bar{\boldsymbol{J}}_B{}^{U}\bar{\boldsymbol{X}}_B \tag{32}$$

Then Eq. (31) can be linearized as

$$\left(\bar{\boldsymbol{M}} + \bar{\boldsymbol{J}}_P^T\bar{\boldsymbol{M}}_s\bar{\boldsymbol{J}}_P\right){}^{U}\ddot{\bar{\boldsymbol{X}}}_P + \bar{\boldsymbol{J}}_P^T\bar{\boldsymbol{B}}\bar{\boldsymbol{J}}_P{}^{U}\dot{\bar{\boldsymbol{X}}}_P + \bar{\boldsymbol{J}}_P^T\bar{\boldsymbol{K}}\bar{\boldsymbol{J}}_P{}^{U}\bar{\boldsymbol{X}}_P = \bar{\boldsymbol{J}}_P^T\bar{\boldsymbol{B}}\bar{\boldsymbol{J}}_B{}^{U}\dot{\bar{\boldsymbol{X}}}_B + \bar{\boldsymbol{J}}_P^T\bar{\boldsymbol{K}}\bar{\boldsymbol{J}}_B{}^{U}\bar{\boldsymbol{X}}_B + \bar{\boldsymbol{F}}_e \tag{33}$$

Equation (33) is the dynamic equation of the vibration isolation platform. If the payload is a rigid spacecraft that is rigidly attached to the PI, the matrix of transmissibility from the LVI to the spacecraft can be written as

$$\bar{\boldsymbol{T}} = {}^{U}\bar{\boldsymbol{X}}_P(s){}^{U}\bar{\boldsymbol{X}}_B(s)^{-1} = (\bar{\boldsymbol{M}}_P s^2 + \bar{\boldsymbol{J}}_P^T\bar{\boldsymbol{B}}\bar{\boldsymbol{J}}_P s + \bar{\boldsymbol{J}}_P^T\bar{\boldsymbol{K}}\bar{\boldsymbol{J}}_P)^{-1}(\bar{\boldsymbol{J}}_P^T\bar{\boldsymbol{B}}\bar{\boldsymbol{J}}_B s + \bar{\boldsymbol{J}}_P^T\bar{\boldsymbol{K}}\bar{\boldsymbol{J}}_B) \tag{34}$$

where $\bar{\boldsymbol{M}}_P = \bar{\boldsymbol{M}}_A + \bar{\boldsymbol{J}}_P^T\bar{\boldsymbol{M}}_s\bar{\boldsymbol{J}}_P$, and $\bar{\boldsymbol{M}}_A$ is the mass and inertia matrix of the PI and the payload.

In the above analysis, the number of struts N is 8. In fact, the analysis procedure is applicable in any case if $N \geq 6$.

C. Parameters of a Symmetric Octostrut Platform

Because the mechanical interfaces of the launch vehicle and the spacecraft are symmetric and circular, it is recommended that the isolation platform should be also a symmetric structure (Fig. 8) with joint points symmetrically placed in two rings with respect to the x and y axes of $\{P\}$. To further simplify the design and analysis of the isolation platform, all struts are assumed to have the same dynamic properties. For the sake of concentrating the discussion on the natural properties of the platform and the spacecraft, the excitation terms in Eq. (33) are omitted, and then this equation can be turned into

$$\left(\bar{\boldsymbol{M}}_A + \bar{\boldsymbol{J}}_P^T\bar{\boldsymbol{M}}_s\bar{\boldsymbol{J}}_P\right){}^{U}\ddot{\bar{\boldsymbol{X}}}_P + \bar{\boldsymbol{J}}_P^T\bar{\boldsymbol{B}}\bar{\boldsymbol{J}}_P{}^{U}\dot{\bar{\boldsymbol{X}}}_P + \bar{\boldsymbol{J}}_P^T\bar{\boldsymbol{K}}\bar{\boldsymbol{J}}_P{}^{U}\bar{\boldsymbol{X}}_P = 0 \tag{35}$$

According to Eq. (24),

$$\bar{\boldsymbol{J}}_P^T\bar{\boldsymbol{K}}\bar{J}_P = \begin{bmatrix} \bar{\boldsymbol{u}}_1 & \cdots & \bar{\boldsymbol{u}}_N \\ \bar{\boldsymbol{s}}_1 & \cdots & \bar{\boldsymbol{s}}_N \end{bmatrix} \begin{bmatrix} k & 0 & \cdots & 0 \\ 0 & k & \cdots & 0 \\ \vdots & \vdots & \ddots & 0 \\ 0 & 0 & \cdots & k \end{bmatrix} \begin{pmatrix} \bar{\boldsymbol{u}}_1^T & \bar{\boldsymbol{s}}_1^T \\ \vdots & \vdots \\ \boldsymbol{u}_N & \bar{\boldsymbol{s}}_N^T \end{pmatrix}$$

$$= k \begin{bmatrix} \sum_{i=1}^{N}\bar{\boldsymbol{u}}_i\bar{\boldsymbol{u}}_i^T & \sum_{i=1}^{N}\bar{\boldsymbol{u}}_i\bar{\boldsymbol{s}}_i^T \\ \sum_{i=1}^{N}\bar{\boldsymbol{s}}_i\bar{\boldsymbol{u}}_i^T & \sum_{i=1}^{N}\bar{\boldsymbol{s}}_i\bar{\boldsymbol{s}}_i^T \end{bmatrix} \tag{36}$$

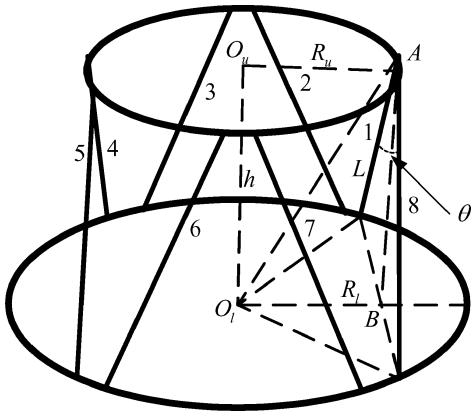

Fig. 8 Symmetric octostrut vibration isolation platform.

where $\bar{s}_i = {}^P\tilde{q}_i\bar{u}_i$. Let $\bar{p}_i = [p_{ix}\ \ p_{iy}\ \ p_{iz}]^T$, $\bar{q}_i = [q_{ix}\ \ q_{iy}\ \ q_{iz}]^T$, $\bar{u}_i = [u_{i1}\ \ u_{i2}\ \ u_{i3}]^T$, and $\bar{s}_i = [s_{i1}\ \ s_{i2}\ \ s_{i3}]^T$. From structural symmetry,

$$\sum_{i=1}^{N} p_{ix} = \sum_{i=1}^{N} p_{iy} = \sum_{i=1}^{N} q_{ix} = \sum_{i=1}^{N} q_{iy} = \sum_{i=1}^{N} p_{ix}p_{iy} = \sum_{i=1}^{N} q_{ix}q_{iy} = \sum_{i=1}^{N} p_{ix}q_{iy} = 0 \tag{37}$$

$$p_{1z} = p_{2z} = \cdots = p_{Nz}, \qquad q_{1z} = q_{2z} = \cdots = q_{Nz} \tag{38}$$

These relations result in

$$\sum_{i=1}^{N} u_{ik}u_{il} = \sum_{i=1}^{N} s_{ik}s_{il} = \sum_{i=1}^{N} {}^{U}u_{ik}s_{il} = 0$$

$$k \quad \text{or} \quad l = 3, \quad \text{and} \quad k \neq l$$

$$\sum_{i=1}^{N} u_{i1}u_{i2} = 0, \qquad \sum_{i=1}^{N} s_{i1}s_{i2} = 0, \qquad \sum_{i=1}^{N} u_{i1}s_{i1} = 0$$

$$\sum_{i=1}^{N} u_{i2}s_{i2} = 0, \qquad \sum_{i=1}^{N} u_{i3}s_{i3} = 0 \tag{39}$$

Thus Eq. (36) can be turned into

$$\bar{J}_P^T\bar{K}\bar{J}_P = k\begin{bmatrix} \sum_{i=1}^{N} u_{i1}^2 & 0 & 0 & 0 & \sum_{i=1}^{N} u_{i1}s_{i2} & 0 \\ 0 & \sum_{i=1}^{N} u_{i2}^2 & 0 & \sum_{i=1}^{N} u_{i2}s_{i1} & 0 & 0 \\ 0 & 0 & \sum_{i=1}^{N} u_{i3}^2 & 0 & 0 & 0 \\ 0 & \sum_{i=1}^{N} s_{i1}u_{i2} & 0 & \sum_{i=1}^{N} s_{i1}^2 & 0 & 0 \\ \sum_{i=1}^{N} s_{i2}u_{i1} & 0 & 0 & 0 & \sum_{i=1}^{N} s_{i2}^2 & 0 \\ 0 & 0 & 0 & 0 & 0 & \sum_{i=1}^{N} s_{i3}^2 \end{bmatrix} \tag{40}$$

There is no coupling stiffness between z-direction displacement and other DOFs. Because $\bar{J}_P^T\bar{B}\bar{J}_P$ and $\bar{J}_P^T\bar{M}_s\bar{J}_P$ have the same form as $\bar{J}_P^T\bar{K}\bar{J}_P$, the dynamic equation along the z axis is independent and can be expressed as

$$\left(m_A + m_s\sum_{i=1}^{N} u_{i3}^2\right){}^{U}\ddot{z}_P + \left(b\sum_{i=1}^{N} u_{i3}^2\right){}^{U}\dot{z}_P + \left(k\sum_{i=1}^{N} u_{i3}^2\right){}^{U}z_P = 0 \tag{41}$$

Equation (41) provides a relation between the parameters of each strut and the platform and those fundamental parameters studied in Sec. II. In Sec. II, it was identified that the desired axial resonant frequency and damping ratio of the platform are 6.5 Hz and 0.19, respectively. According to Eq. (41), for an octostrut platform whose structural parameters are listed in Table 3 (same interface dimension as the original PAF) and the same spacecraft as used in Sec. II, the stiffness of the spring and the damping ratio of a single strut are calculated as 7.9534×10^5 N/m and 5842.3 kg/s, respectively.

For a slender spacecraft, to achieve better isolation performance, the isolation platform is softer and thus the rotational stiffness of the platform is usually low. This may lead to a large lateral displacement of the upper end of the spacecraft and results in its collision with the fairing. To prevent this from happening, a constraint mechanism can be placed along with the platform. With the constraint mechanism, only three translational DOFs are left. All rotational DOFs are restrained, but they have no effects on the vibration along the axial direction of the LV. The natural frequencies of the vibration isolation system with or without a constraint mechanism are listed in Table 4.

To test the redundancy characteristics of the octostrut platform, one strut is assumed to have failed by setting its stiffness to zero. The natural frequencies of the isolation system with this failure are also listed in Table 4. When it is compared with the normal system, the structure of the platform is kept, although two natural frequencies decrease slightly.

IV. Coupling Dynamics

In the preliminary analysis, the LV, the spacecraft, and the platform are modeled only as a five-DOF system. It can only represent the main characteristics of the LV and the spacecraft along the longitudinal axis and cannot account for all of their dynamic behavior. In this section, the LV and the spacecraft are modeled as a finite element model. Because of fuel depletion and stage jettisons, the LV changes significantly during its ascent, but it is too tedious here to report results at every second. Therefore, only three typical flight events were selected as examples, liftoff, the first-stage separation, and the second-stage separation. FEMs are built for each event. The fundamental parameters of the LV selected in this paper are in Table 1. The FEM of the LV at the liftoff has 6832 elements. To integrate the FEMs of the LV and the spacecraft, the platform should also be modeled as a FEM. Each strut of the platform is modeled as a single-direction spring with damper.

Transfer functions between main-engine force input and spacecraft acceleration output are used to estimate the performance of the platform. The original cone-shaped stiff PAF is also computed with the above FEMs of the LV and the spacecraft. Figures 9–14 show curves of the transfer function at given stages and in given directions, in which solid lines indicate the transfer function with the original PAF, dotted lines indicate the transfer function with the vibration isolation platform, and dash-dotted lines indicate the transfer function with the one-strut-failed platform. As a feature of vibration isolation, these curves show that around the first natural coupling frequency of the platform and the spacecraft, vibration is amplified, whereas vibrations above this frequency are significantly

Table 3 Structural parameters of the platform

Up platform radius	Low platform radius	Platform height	Included angle of a pair of struts	Upper joint distant of a pair of struts
$R_u = 0.607$	$R_l = 0.874$	$h = 0.65$	$\theta = 5\pi/12$	$l_d = 0.05$

Table 4 Nature of frequencies of the vibration isolation platform and the rigid spacecraft

Work condition	Natural frequency, Hz					
Without constraint	1.7175	1.7392	3.0343	4.6177	4.7457	6.5000 (axial)
With constraint	2.9906	2.9906	6.5000 (axial)			
With constraint (one strut failed)	2.5145	2.9906	6.1118			

Table 5 Summary of isolation performance (rms ratio)

Direction	Liftoff	First-stage separation	Second-stage separation
Along z axis (lateral)	0.424	0.141	0.133
Along x axis (axial)	0.701	0.106	0.454

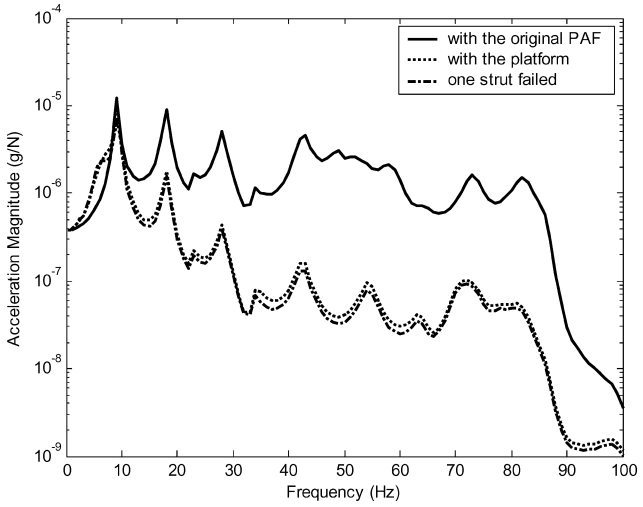

Fig. 9 Longitudinal transfer function from the nozzle to the bottom of the spacecraft at the liftoff.

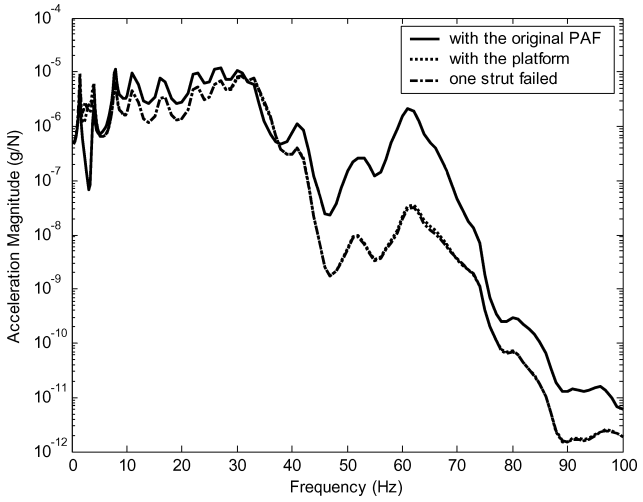

Fig. 10 Lateral transfer function from the nozzle to the bottom of the spacecraft at the liftoff.

attenuated. And because of the redundancy of the octoplatform, the one-strut fault has little effect on the isolation performance of the platform. The ratios of the rms of the isolated acceleration power spectral density (PSD) to the rms of the nonisolated acceleration PSD are computed in Table 5. The rms ratio along the z axis decreases with the stage separation, but that along the x axis does not monotonically decrease. As a whole, the multistrut passive vibration isolation platform is an effective method for attenuating loads on the spacecraft.

For a launch vehicle provider, to guarantee flight stability of the vehicle control system, changes in the dynamic properties brought about by the replacement of the original PAF with the vibration isolation platform is most concerned. Two main factors often considered are natural frequencies and mode shapes. Table 6 lists natural frequencies of some beam-like modes and new modes caused by the platform. At the liftoff and the first-stage separation, the vibration isolation platform causes three new modes, and the original modes are nearly unchanged. To scale the mode-shape variation of these common modes, their mode-shape

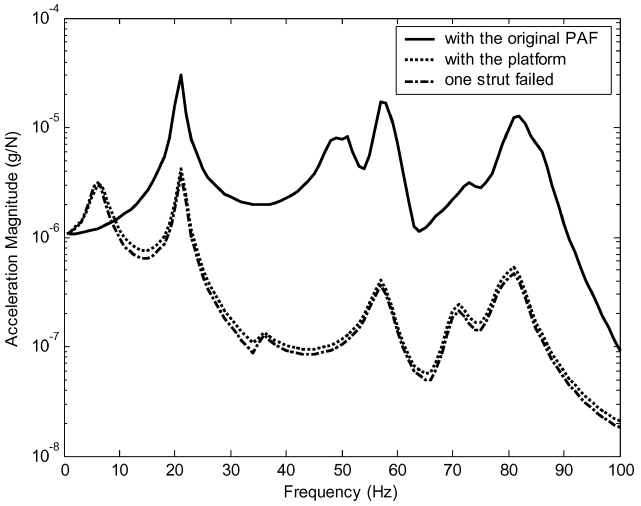

Fig. 11 Longitudinal transfer function from the nozzle to the bottom of the spacecraft at the first-stage separation.

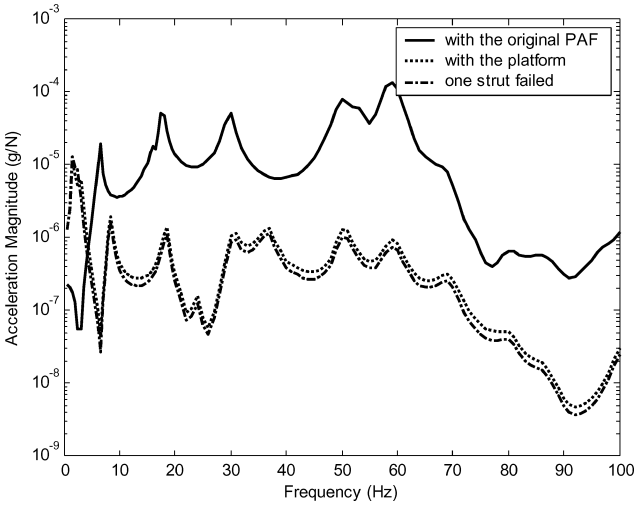

Fig. 12 Lateral transfer function from the nozzle to the bottom of the spacecraft at the first-stage separation.

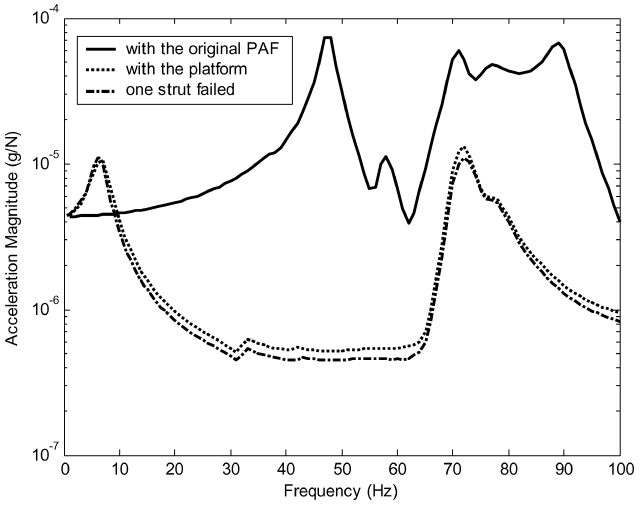

Fig. 13 Longitudinal transfer function from the nozzle to the bottom of the spacecraft at the second-stage separation.

Table 6 Natural frequencies of the launch vehicle–platform–spacecraft structure[a]

Liftoff			First-stage separation			Second-stage separation		
Original PAF	Isolation platform	MSCC	Original PAF	Isolation platform	MSCC	Original PAF	Isolation platform	MSCC
1.45(L)	1.45(L)	0.99999						
	3.05(L)			3.05(L)			4.14(L)	
3.91(L)	3.91(L)	0.99999	6.35(L)	6.35(L)	0.99999			
	6.42(A)			6.57(A)			6.87(A)	
7.89(L)	7.89(L)	0.99999	17.65(L)	17.59(L)	0.99994	17.83(L)		
9.10(A)	9.34(A)	0.99977	20.88(A)	21.20(A)	0.99970		32.136(L)	
11.34(L)	11.34(L)	0.99994	29.79(L)	29.87(L)	0.99995	37.24(L)		

[a]L denotes lateral vibration mode. For near symmetry of the LV and the spacecraft, there are two modes for each natural frequency with L. A denotes axial vibration mode. R denotes rotation vibration mode along the axis of the LV.

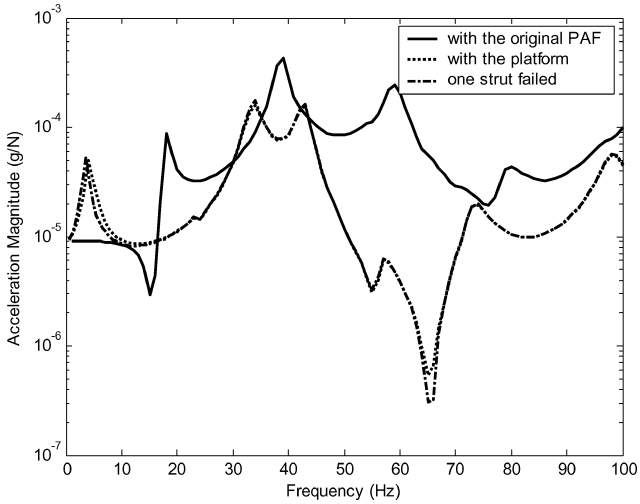

Fig. 14 Lateral transfer function from the nozzle to the bottom of the spacecraft at the second-stage separation.

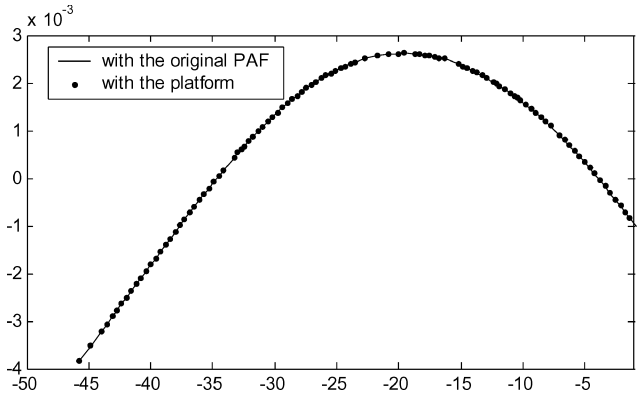

Fig. 15 Mode shape of the first lateral mode.

correlation coefficients (MSCCs) are calculated. These are defined as

$$\mathrm{MSCC} = \frac{\left|\bar{\varphi}_n^T \bar{\psi}_r\right|}{|\bar{\varphi}_n||\bar{\psi}_r|} \tag{42}$$

where $\bar{\varphi}_n$ is the mode shape of the LV with the original PAF and $\bar{\psi}_r$ is the mode shape of the LV with the isolation platform. All MSCCs at the liftoff and the first-stage separation are near 1, which means that the replacement with the platform also has little effect on the mode shapes of the LV at these instants. Figure 15 shows mode shapes of the LV part at 1.45 Hz. Two mode shapes nearly coincide. But at the second-stage separation, the vibration modes of different cases are considerably different. The resonant frequencies of the platform coupling with the spacecraft increase greatly and differences among other modes are large. In other words, in this scenario, changes in the dynamic properties of the LV cannot be neglected and their influence on the stability of the vehicle control system should be examined. If the stability cannot be ensured, the isolation performance has to be sacrificed, usually by increasing the resonant frequency of the platform coupled with the spacecraft.

V. Summary

Replacing the original stiff PAF with an octostrut passive vibration isolation platform is an effective and practical method for improving the dynamic environment that a launch vehicle can provide to its payload. To ensure the performance of a platform, dynamic design is most important. The procedure for dynamic design developed in the preceding sections can be summarized as follows:

1) Defining the resonant frequency and damping ratio of the whole platform coupled with the spacecraft. The LV–platform–spacecraft structure is represented by a lumped-parameter model. Loads during the launch are simulated by solving the orbit dynamic equation and applied to the vibration equation. To solve the vibration equation with different resonant frequencies and damping ratios of the platform, time histories of acceleration are calculated. By minimizing RMS acceleration of spacecraft, an optimal resonant frequency and damping ratio pair can be gained for the whole platform.

2) Determining the parameters of each strut. From the dynamic equation of the platform, for a given platform structure, the stiffness and damping coefficient of a single strut can be determined according to the optimal resonant frequency and the optimal damping ratio of the platform.

3) Coupling analysis. FEMs of the octostrut platform, the spacecraft, and the launch vehicle are put together as a whole structure. The transfer function between main-engine force input and spacecraft acceleration output at interesting instants is calculated to estimate the performance of the platform, and natural frequencies and mode shapes are computed and compared to those with the original PAF to estimate the influence of the platform on the dynamic properties of the launch vehicle.

The example in Sec. IV shows that at the liftoff and the first-stage separation, the replacement of the PAF with the platform has a negligible effect on the dynamic properties of the LV, but at the second-stage separation, changes in the dynamic properties of the LV cannot be neglected. Therefore, possible influences of the platform on the stability of the vehicle control system should be examined.

References

[1]Johnson, C. D., Wilke, P. S., and Darling, K. R., "Multi-Axis Whole-Spacecraft Vibration Isolation for Small Launch Vehicles," *Proceedings of Smart Structures and Materials*, Vol. 4331, Society of Photo-Optical Instrumentation Engineers, Bellingham, WA, 2001, pp. 153–161.

[2]Wilke, P. S., and Johnson, C. D., "Whole-Spacecraft Passive Launch Isolation," *Journal of Spacecraft and Rockets*, Vol. 35, No. 5, 1998, pp. 690–694.

[3]Denoyer, K. K., and Johnson, C. D., "Recent Achievements in Vibration Isolation Systems for Space Launch and On-Orbit Application," 52nd International Astronautical Congress, 2001.

[4]Edberg, D. L., and Johnson, C. D., "On the Development of a Launch Vibration Isolation System," *Proceedings of Smart Structures*, Vol. 3045, Society of Photo-Optical Instrumentation Engineers, Bellingham, WA, 1997, pp. 31–37.

[5]Geng, Z. J., and Haynes, L. S., "Six Degree-of-Freedom Active Vibration Control Using the Stewart Platforms," *IEEE Transactions on Control Systems Technology*, Vol. 2, No. 1, 1994, pp. 45–53.

[6]Dasgupta, B., and Mruthyunjaya, T. S., "Closed-Form Dynamic Equations of the General Stewart Platform Through the Newton–Euler Approach," *Mechanism and Machine Theory*, Vol. 33, No. 7, 1998, pp. 993–1012.

[7]McInroy, J. E., and Hamann, J. C., "Design and Control of Flexure Jointed Hexapods," *IEEE Transactions on Robotics and Automation*, Vol. 16, No. 4, 2000, pp. 372–381.

[8]McInroy, J. E., "Modeling and Design of Flexure Jointed Stewart Platforms for Control Purposes," *IEEE/ASME Transactions on Mechatronics*, Vol. 7, No. 1, 2002, pp. 95–99.

[9]Karahalis, G. G., and Agnes, G. S., "Preliminary Analysis of Hybrid Launch Isolation for Spacecraft," *Proceedings of Smart Structures*, Vol. 3674, Society of Photo-Optical Instrumentation Engineers, Bellingham, WA, 1999, pp. 360–370.

[10]Karahalis, G. G., "Whole Spacecraft Vibration Isolation," M.S. Thesis, School of Engineering, Air Force Inst. of Technology, Wright–Patterson AFB, OH, March 1999.

[11]Wiesel, W. E., *Spaceflight Dynamics*, Irwin/McGraw–Hill, New York, 1989, pp. 207–211.

L. Peterson
Associate Editor